



# A localized adaptor protein performs distinct functions at the *Caulobacter* cell poles

Jiarui Wang<sup>a,b</sup>, W. E. Moerner<sup>a,c,1</sup>, and Lucy Shapiro<sup>b,c,1</sup>

<sup>a</sup>Department of Chemistry, Stanford University, Stanford, CA 94305; <sup>b</sup>Department of Developmental Biology, Stanford University School of Medicine, Stanford, CA 94305; and <sup>c</sup>Chan Zuckerberg Biohub, San Francisco, CA 94158

Contributed by Lucy Shapiro, February 8, 2021 (sent for review November 30, 2020; reviewed by Johan Elf and Arash Komeili)

**Asymmetric cell division generates two daughter cells with distinct characteristics and fates. Positioning different regulatory and signaling proteins at the opposing ends of the predivisional cell produces molecularly distinct daughter cells. Here, we report a strategy deployed by the asymmetrically dividing bacterium *Caulobacter crescentus* where a regulatory protein is programmed to perform distinct functions at the opposing cell poles. We find that the CtrA proteolysis adaptor protein PopA assumes distinct oligomeric states at the two cell poles through asymmetrically distributed c-di-GMP: dimeric at the stalked pole and monomeric at the swarmer pole. Different polar organizing proteins at each cell pole recruit PopA where it interacts with and mediates the function of two molecular machines: the ClpXP degradation machinery at the stalked pole and the flagellar basal body at the swarmer pole. We discovered a binding partner of PopA at the swarmer cell pole that together with PopA regulates the length of the flagella filament. Our work demonstrates how a second messenger provides spatio-temporal cues to change the physical behavior of an effector protein, thereby facilitating asymmetry.**

asymmetry | single-particle tracking | second messenger | flagellar assembly | protein degradation

Asymmetric cell division, which yields daughter cells with different morphologies and cell fates, underlies stem cell behavior and cellular diversity in all organisms (1, 2). One path to enable asymmetric cell division requires the predivisional cell to dynamically position different regulatory proteins to opposite sides of the cell or at opposing cell poles (2–5). Another strategy uses symmetrically distributed proteins at the two cell poles that perform spatially defined asymmetric functions yielding daughter cells exhibiting distinct behaviors (6–10). Using multifunctional proteins that act differently at distinct locations within the cell is a strategy in eukaryotic cells as well. For example, dual-function  $\beta$ -catenin forms a complex with cadherin at the membrane to regulate cell–cell adhesion (11, 12), while upon translocation to the nucleus it functions to control transcription (13). Here, we have defined the mechanism for a symmetrically localized regulatory protein in the predivisional cell of the bacterium *Caulobacter crescentus* to carry out different functions at spatially distinct sites.

The bacterium *Caulobacter crescentus* has proven to be a useful model organism that yields two distinct daughter cells at every division (14, 15). Each division produces a motile swarmer cell, incapable of DNA replication, and a stationary stalked cell that can immediately enter the next cell cycle (15) (Fig. 1A). In order to divide, the swarmer cell has to first differentiate into a stalked cell by shedding its flagellum and pili and assembling a stalk at the same pole (14) (Fig. 1A). The cell then makes the critical decision to initiate DNA replication (15). As the chromosome is being replicated and segregated to two daughter compartments prior to division, a new flagellum is synthesized at the pole opposite the stalk (15) (Fig. 1A).

A key element controlling cellular asymmetry involves the spatiotemporal activation and degradation of the CtrA master transcription factor (16), which directly controls the expression of over 90 genes (17) and also blocks the chromosomal origin of

replication (18). One critical event takes place as the cell decides to divide: CtrA, present throughout most of the cell cycle, is cleared from the cell during the swarmer-to-stalked transition and in the stalked compartment of the predivisional cell, thus confining the initiation of DNA replication to only the stalked cells (16, 19, 20). Additional mechanisms control *ctrA* transcription and translation, which peak in the predivisional cell (18) and regulate CtrA activation by phosphorylation (16). The robust control of the asymmetric abundance of CtrA and the cell cycle timing of CtrA activation yield differential readout of the chromosome in the two daughter cells (15).

The proteolysis of CtrA occurs only at the stalked pole and requires a cyclic-di-GMP binding protein, PopA (21–24), which is the primary focus of this paper. During the swarmer-to-stalked cell transition and in late predivisional cells, a ClpXP protease complex localizes to the stalked pole along with three adaptor proteins, CpdR, RcdA, and PopA, that prime the protease for substrate recognition (25, 26). PopA directly recruits CtrA to the ClpXP protease for degradation (22). Surprisingly, while critical for the development of asymmetry, PopA symmetrically localizes to both cell poles throughout the cell cycle (21), even though no other part of the degradation complex (ClpX, ClpP, CpdR, and RcdA) is symmetrically localized (26).

Duerig et al. (21) showed that the binding of PopA to c-di-GMP specifically modulates PopA's localization and function at the stalked but not the flagellated swarmer pole. In *Caulobacter*, the synthesis and destruction of c-di-GMP occurs at opposite poles (15): The primary diguanylate cyclase PleD that synthesizes

## Significance

**Asymmetric cell division yields two distinct daughter cells by mechanisms that underlie stem cell behavior and cellular diversity in all organisms. The bacterium *Caulobacter crescentus* is able to orchestrate this complex process with less than 4,000 genes. This article describes a strategy deployed by *Caulobacter* where a regulatory protein, PopA, is programmed to perform distinct roles based on its subcellular address. We demonstrate that, depending on the availability of a second messenger molecule, PopA adopts either a monomer or dimer form. The two oligomeric forms interact with different partners at the two cell poles, playing a critical role in the degradation of a master transcription factor at one pole and flagellar assembly at the other pole.**

Author contributions: J.W., W.E.M., and L.S. designed research; J.W., W.E.M., and L.S. performed research; W.E.M. and L.S. contributed new reagents/analytic tools; J.W., W.E.M., and L.S. analyzed data; and J.W., W.E.M., and L.S. wrote the paper.

Reviewers: J.E., Uppsala University; and A.K., University of California, Berkeley.

The authors declare no competing interest.

This open access article is distributed under [Creative Commons Attribution-NonCommercial-NoDerivatives License 4.0 \(CC BY-NC-ND\)](https://creativecommons.org/licenses/by-nc-nd/4.0/).

<sup>1</sup>To whom correspondence may be addressed. Email: wmoerner@stanford.edu or shapiro@stanford.edu.

This article contains supporting information online at <https://www.pnas.org/lookup/suppl/doi:10.1073/pnas.2024705118/-/DCSupplemental>.

Published March 22, 2021.

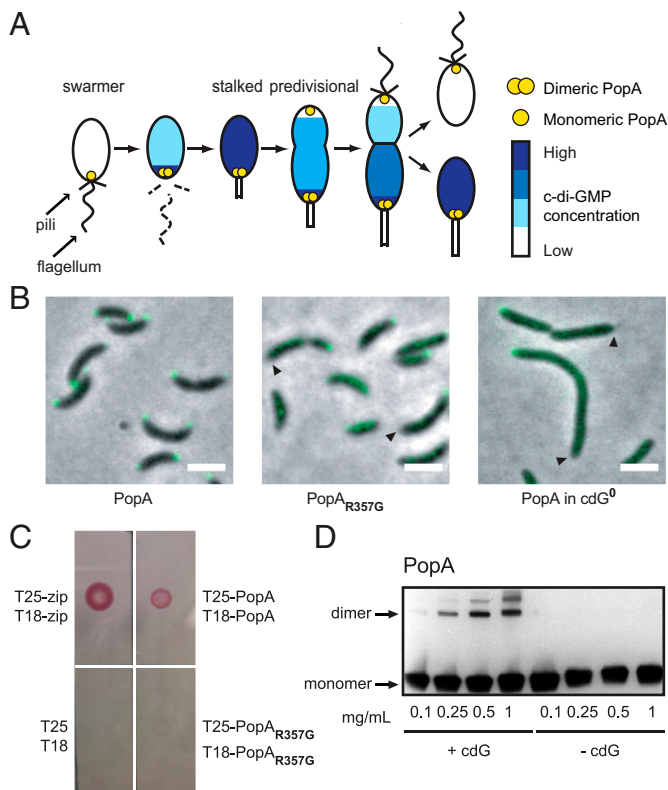


**Fig. 1.** PopA subcellular distribution and proposed c-di-GMP-dependent oligomeric states. (A) Schematic of the *Caulobacter crescentus* cell cycle yielding a swarmer cell and a stalked cell upon division. The second messenger c-di-GMP (blue) is asymmetrically distributed, with low levels in motile swarmer cells and high levels in stalked cells (29). The swarmer cell cannot initiate DNA replication until it differentiates into a stalked cell by shedding its flagellum and pilus and building a stalk at the same site. De novo synthesis of c-di-GMP initiates during the swarmer-to-stalked cell transition, reaching peak concentration in stalked cells. The biogenesis of a new flagellum occurs at pole opposite the stalk. PopA (yellow circles) regulates the degradation of the master regulator CtrA at the stalked pole by ClpXP (21) yet is positioned at both cell poles. We propose that PopA adopts distinct oligomeric states at the opposing cell poles in response to local c-di-GMP concentration, dimeric at the stalked pole and monomeric at the opposite pole. (B) Subcellular localization of PopA-eYFP in a WT genetic background and in a mutant strain unable to synthesize c-di-GMP ( $cdG^0$ ), and localization of a mutant of PopA<sub>R357G</sub>-eYFP unable to bind c-di-GMP. In the absence of c-di-GMP, PopA fails to localize to the stalked pole but is retained at the opposite pole. The chromosomal *popA* locus was replaced with either *popA-eyfp* or with *popA<sub>R357G</sub>-eyfp*. Black arrowheads indicate the stalked pole in the phase-fluorescence merged images. (Scale bars: 2  $\mu$ m.) Ninety-two percent, 5%, and 11% of WT, PopA<sub>R357G</sub>, and  $cdG^0$  cells, respectively, have bipolar foci (calculated for 212, 110, and 122 predivisional cells). (C) BacTH assays showed self-association of PopA (21) but not PopA<sub>R357G</sub>-PopA<sub>R357G</sub> in vivo. (D) Cross-link assays showed that c-di-GMP induces PopA dimerization in vitro. Purified PopA (0.1, 0.25, 0.5 and 1 mg/mL) with or without c-di-GMP was incubated with 2.5 mM BS3 (Abcam) for 30 min. PopA monomers and dimers were separated on an SDS-PAGE gel (equal amount of total protein was loaded into each lane), transferred to PVDF membranes, and detected by immunoblot analysis with an anti-PopA antibody. The arrows mark the monomeric and dimeric forms of PopA.

c-di-GMP is sequestered to the stalked pole (27), while the primary phosphodiesterase PdeA that degrades c-di-GMP is concentrated at the swarmer pole (14, 15, 28), giving rise to an asymmetric distribution of c-di-GMP (29) (Fig. 1A, blue shading).

We provide in vivo and in vitro evidence that PopA assumes distinct oligomeric states at the opposing poles and that the difference in oligomeric states of PopA enables its functional asymmetry (Fig. 1A). By single-molecule diffusion analysis and bimolecular

fluorescence complementation (BiFC), we show that in vivo PopA dimerizes in the presence of c-di-GMP and preferentially forms PopA dimers at the stalked pole. Moreover, PopA's polar localization depends on interaction with different polar organizing proteins: PodJ at the swarmer pole and PopZ at the stalked pole. We discovered a binding partner of PopA at the swarmer pole that together with PopA regulates flagellar filament length. We propose that the asymmetric distribution of c-di-GMP drives PopA into two populations that mediate the function of two different molecular machines—the flagellar basal body at the swarmer pole and the ClpXP degradation machinery at the stalked pole.

## Results

**Cyclic-di-GMP Promotes PopA Dimerization In Vitro.** PopA is a structural homolog of the diguanylate cyclase PleD and binds c-di-GMP with an equilibrium dissociation constant  $K_d$  of  $\sim 2 \mu$ M in vitro (21). A single amino acid mutation within the binding pocket of the GGDEF domain, R357G, prevents PopA from binding to c-di-GMP (21). As previously published, PopA<sub>R357G</sub>-eYFP localizes to only the swarmer pole, as opposed to the symmetric distribution to both poles in wild-type (WT) cells, and cannot assist ClpXP in CtrA degradation (21) (Fig. 1B, Center). In a cell line completely lacking c-di-GMP ( $cdG^0$ ), PopA-eYFP only forms a single focus at the swarmer pole (30) (Fig. 1B, Right). These observations suggest that PopA employs two distinct mechanisms to target the opposing cell poles: a c-di-GMP-dependent mechanism at the stalked pole and a c-di-GMP-independent mechanism at the swarmer pole.

We considered the possibility that c-di-GMP controls the polar localization of PopA through dimerization. A weak self-association of PopA in *Escherichia coli* using a bacterial two-hybrid (BacTH) system has been reported (21). We reproduced PopA self-association using the BacTH system. Furthermore, we found that the mutant PopA<sub>R357G</sub>, which does not bind c-di-GMP, failed to self-associate (Fig. 1C). It was previously reported that  $0.31 \mu$ M intracellular c-di-GMP is present in *E. coli* (31). The nonpolar intracellular c-di-GMP levels in *Caulobacter* were estimated to fluctuate between 0 (swarmer cells) to  $0.5 \mu$ M (stalked cells) during the cell cycle (29). This difference in self-association observed for PopA and PopA<sub>R357G</sub> in *E. coli* suggested that PopA-PopA interaction could be c-di-GMP dependent. To verify that PopA self-association is driven by c-di-GMP, we performed cross-linking studies with purified PopA using chemical cross-linker BS3 (Bis-sulfosuccinimidyl suberate) (Fig. 1D). Cross-linked PopA dimers appeared upon the addition of c-di-GMP. The dimeric population of PopA increased as the PopA concentration was increased (Fig. 1D). Schalch-Moser (32), a student in the Urs Jenal laboratory (University of Basel, Basel, Switzerland), documented a nondenaturing gel electrophoresis experiment in her thesis showing that PopA dimerization increased as a function of c-di-GMP concentration in vitro.

## PopA Diffuses as a Smaller Complex in the Absence of c-di-GMP.

Next, we assessed c-di-GMP-dependent dimerization in vivo using a diffusion-based estimate of sizes of the diffusing molecules (33–35). According to the Stokes–Einstein equation (Eq. 1), the diffusion coefficient of spherical particles undergoing Brownian diffusion,  $D$ , senses the hydrodynamic radius ( $R_h$ ) and viscosity of the solution ( $\eta$ ) (36, 37). Proteins in different oligomeric states, but in the same cellular environment, hence, should exhibit different diffusion coefficients. The PopA polar foci are made up by mostly immobilized PopA molecules; however, there is a diffuse cytoplasmic population of PopA that shuttles between the two polar regions in the cell body. By analyzing the behavior of the diffusive PopA, we were able to isolate the impact of c-di-GMP on PopA diffusion. Using live-cell single-particle tracking with 20-ms exposures, we measured the apparent early-time diffusion coefficients of PopA-eYFP (77 kDa), the PopA<sub>R357G</sub>-eYFP mutant unable to bind c-di-GMP in a WT background, and PopA-eYFP in a

strain ( $cdG^0$ ) completely depleted of c-di-GMP (30) to evaluate the effect of c-di-GMP on oligomeric states of PopA (Fig. 1B):

$$D = \frac{k_B T}{6\pi\eta R_h} \quad [1]$$

In order to avoid the confounding effect of the variation in cell cycle, we first collected trajectories of PopA proteins in predivisional cells outside the polar region. The ensemble early-time diffusion coefficient for PopA was calculated by analyzing the mean-square displacement (MSD) from pooled trajectories (Fig. 2A). The average diffusion coefficient for PopA-eYFP in a WT background was  $0.615 \pm 0.0176 \mu\text{m}^2/\text{s}$  (error is SD determined from 20 bootstrapped samples of individual tracks) (Fig. 2B). The diffusion coefficients of PopA<sub>R357G</sub>-eYFP in an otherwise WT background and PopA-eYFP in  $cdG^0$  background were  $0.785 \pm 0.0109$  and  $1.01 \pm 0.0144 \mu\text{m}^2/\text{s}$ , respectively (Fig. 2B). The slower diffusion of PopA-eYFP in a background with WT levels of c-di-GMP suggests that it is diffusing as a bigger complex.

The difference in diffusion coefficients of PopA<sub>R357G</sub>-eYFP and PopA-eYFP in  $cdG^0$  (both representing PopA without interaction with c-di-GMP) prompted us to investigate the effective cellular viscosity of the three cell lines in order to infer information about the hydrodynamic radii. The Stokes–Einstein equation (Eq. 1) suggests that if we track the same noninteracting test particle in various cell lines, the difference in diffusion coefficient would reflect the difference in cellular viscosity. We therefore performed a control based on single-particle tracking and MSD analysis of free HaloTag protein (33 kDa) labeled with JF549 in these three isogenic cell lines (WT, WT bearing a PopA<sub>R357G</sub> variant, and a  $cdG^0$  strain) and extracted the relative viscosities to be  $1.00 \pm 0.008$ ,  $0.972 \pm 0.010$ , and  $0.812 \pm 0.018$ , respectively (SI Appendix, Fig. S1). The low cellular viscosity of  $cdG^0$  cells may be accounted for by the fact that these cells demonstrate strong morphological abnormalities (Fig. 1B) with the cells being elongated and erratically shaped (30).

After taking into account the differences in cellular viscosity, the measured diffusion coefficients suggest that the relative hydrodynamic radii of PopA-eYFP, PopA<sub>R357G</sub>-eYFP, and PopA-eYFP in a  $cdG^0$  background are  $1.00 \pm 0.0287$ ,  $0.806 \pm 0.0111$ , and  $0.752 \pm 0.0106$ , respectively, values that can be cubed to obtain estimates of the relative molecular weights:  $1.00 \pm 0.0869$ ,  $0.524 \pm 0.0218$ , and  $0.426 \pm 0.017$  (Fig. 2C, left and right axes, respectively). Since PopA<sub>R357G</sub> is unable to bind c-di-GMP, and  $cdG^0$  cells completely lack c-di-GMP, the relative molecular weights support the possibility that WT PopA dimerizes in the presence of c-di-GMP, leading to slower diffusion (Fig. 2D). The c-di-GMP concentration in *Caulobacter* was previously measured by a fluorescence resonance energy transfer-based sensor to be around 500 nM in predivisional cells (29). The fact that we were able to detect such a clear difference in the ensemble diffusion indicates that the  $K_d$  of PopA binding c-di-GMP in vivo is likely smaller than what was measured in vitro using binding assays.

The c-di-GMP concentration fluctuates during the cell cycle. The swarmer cell has minimum cytosolic c-di-GMP. The synthesis of c-di-GMP begins during the swarmer-to-stalked transition leading to peak c-di-GMP concentrations in stalked cells (29) (Fig. 1A). We performed single-particle tracking in swarmer and stalked cells isolated from synchronized populations of cells to determine the cytoplasmic diffusional behavior of PopA-eYFP in low and high c-di-GMP environments using pooled MSD analysis as above. After correcting for different viscosities of two cell types (SI Appendix, Fig. S2), we estimated the relative hydrodynamic radii of PopA-eYFP, which can be cubed to estimate relative molecular weights of  $0.448 \pm 0.0289$  and  $1.00 \pm 0.0582$  for swarmer and stalked cells, respectively (Fig. 2E). Since the c-di-GMP concentration peaks in the stalked cells and reaches a

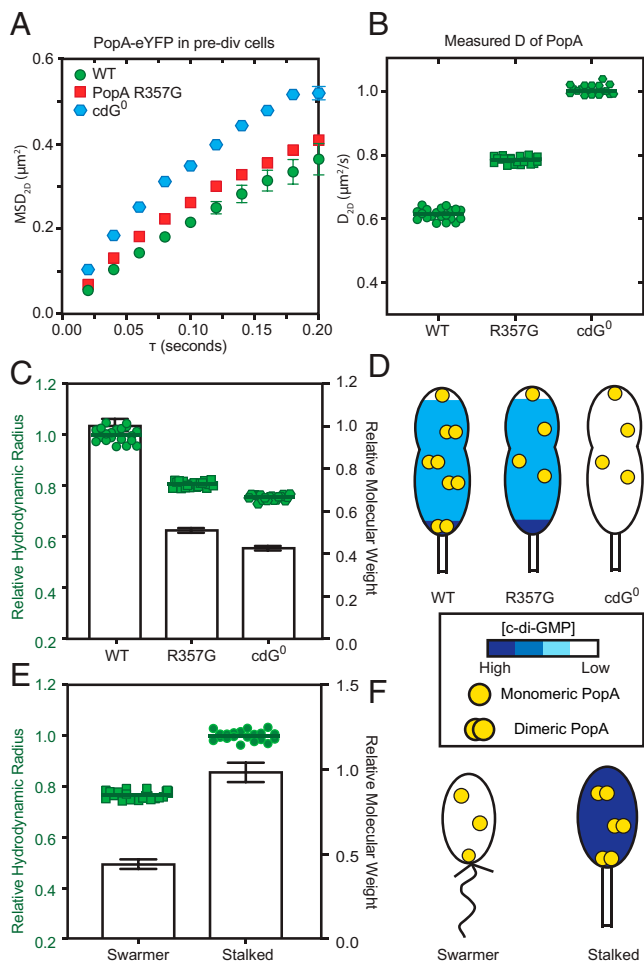


**Fig. 2.** PopA diffuses as a smaller complex in the absence of c-di-GMP. (A) Two-dimensional mean-square displacement (MSD) curves for WT PopA-eYFP (green circles), a mutant PopA<sub>R357G</sub>-eYFP unable to bind c-di-GMP (red squares), and PopA-eYFP in  $cdG^0$  (blue hexagons) pooled trajectories outside the poles. Error bars represent SD calculated from 20 bootstrapped samples. (B) Apparent diffusion coefficients  $D_{2D}$  of PopA-eYFP (circles), PopA<sub>R357G</sub>-eYFP (squares), and PopA-eYFP in  $cdG^0$  (hexagons) for 138, 329, and 387 cells. Each point in the scatter plot comes from one bootstrapped sample, and the bar is the mean of 20 bootstrapped samples. (C) Relative hydrodynamic radii of PopA-eYFP, PopA<sub>R357G</sub>-eYFP, and PopA-eYFP in  $cdG^0$  after correcting for differences in cellular viscosity are plotted in scatter points (each point represents a single bootstrapped sample and bar as mean) as read from the left-side y axis. The corresponding relative molecular weights for PopA-eYFP are shown in bar graphs (right-side y axis), and the error bars represent SD of 20 bootstrapped samples. (D) Proposed PopA-eYFP (yellow circles) oligomeric states (immobile polar populations and diffusive nonpolar population) in predivisional cells as a function of c-di-GMP concentration (blue shading). (E) Relative hydrodynamic radii of PopA-eYFP in swarmer and stalked cells (206 and 491 cells) after correcting for difference in cellular viscosity are plotted in scatter points (each point represents a single bootstrapped sample and bar as mean) and read off left-side y axis. The corresponding relative molecular weights for PopA-eYFP are shown in bar graphs (right-side y axis), and the error bars represent SD of 20 bootstrapped samples. (F) Proposed PopA-eYFP (yellow circles) oligomeric states (immobile polar population and diffusive nonpolar population) in swarmer vs. stalked cells that have low and high concentration of c-di-GMP (blue shading).

minimum in the swarmer cells, our measurements support the hypothesis that PopA-eYFP dimerizes in the presence of c-di-GMP in *Caulobacter* (Fig. 2F).

**PopA Preferentially Dimerizes at the Stalked Pole.** To directly visualize the dimerization of PopA within the polar regions in vivo,

we implemented a BiFC assay (38). We divided eYFP into two nonfluorescent fragments, eYFP<sup>N</sup> and eYFP<sup>C</sup>, as described by Kerppola (38), and fused them to the C-terminal ends of PopA or to PopA<sub>R357G</sub> that cannot bind to c-di-GMP (Fig. 3A). Fluorescent signal would indicate PopA dimerization. We then introduced either PopA-eYFP<sup>N</sup>/PopA-eYFP<sup>C</sup> or PopA<sub>R357G</sub>-eYFP<sup>N</sup>/PopA<sub>R357G</sub>-eYFP<sup>C</sup> into a  $\Delta popA$  deletion strain. We were able to detect fluorescent signals from dimeric PopA-eYFP<sup>N</sup>/PopA-eYFP<sup>C</sup> predominantly at the stalked pole, demonstrating PopA dimerization in vivo (Fig. 3B). No fluorescence was detected in the cells containing the PopA<sub>R357G</sub>-eYFP<sup>N</sup>/PopA<sub>R357G</sub>-eYFP<sup>C</sup> constructs, suggesting that it was the PopA/PopA interaction but not the eYFP<sup>N</sup>/eYFP<sup>C</sup> interaction that drove the dimerization (SI Appendix, Fig. S3). In addition, we quantified the fluorescence complementation in predivisional cells, as PopA are bipolarly localized in these cells. We measured the fluorescence intensity ratio of BiFC at the stalked pole vs. the swarmer pole. Less than 19.5% of the cells (ST-to-SW BiFC signal is at or below 1) exhibit higher fluorescence signal at the swarmer pole (514 cells), while most cells show stronger BiFC signal at the stalked pole (Fig. 3C). Upon chromophore maturation, the eYFP fragments stay as a stable complex (39). Therefore, the fluorescence complementation observed at the swarmer pole could be caused by a small fraction of previously formed PopA dimers. Our results showed that in vivo PopA dimerizes in a c-di-GMP-dependent manner, and dimeric PopA preferentially localizes to the stalked pole.

**PopA Targets the Opposing Poles through Different Polar Organizing Proteins.** We now dissect the mechanisms that target PopA to the two distinct cell poles. PodJ functions as a polar organizing protein upon its localization to the flagella-bearing pole of the swarmer cell (40–42). Consistent with Duerig et al., rather than localizing in a bipolar pattern, in 81% of predivisional cells PopA loses its swarmer pole foci in a  $\Delta podJ$  strain (21, 22) (Fig. 4A), suggesting that PodJ recruits PopA to the swarmer pole. To determine whether PodJ interacts with PopA, we performed a BacTH assay by expressing PopA/PodJ and PopA<sub>R357G</sub>/PodJ in *E. coli*. Both PopA and PopA<sub>R357G</sub> interacted with PodJ in this assay (Fig. 4B, middle column). Thus, in this heterologous test, the PopA–PodJ interaction is c-di-GMP independent and thus consistent with the observation (Fig. 1B) that PopA<sub>R357G</sub>-eYFP localizes to the *Caulobacter* swarmer pole and with recent work that also shows a positive interaction between PodJ and PopA using heterologous reconstitution (42).

PopZ is a polar organizing protein that forms a membraneless microdomain at the stalked pole and at the swarmer pole in the predivisional cells (43–47). By concentrating distinct client

proteins at the cell poles, PopZ maintains cellular asymmetry during division (44, 48, 49). Ozaki et al. showed that PopA only formed a single focus at the swarmer pole in  $\Delta popZ$  strain and became completely diffuse in a  $\Delta podJ \Delta popZ$  double deletion (21, 22). We also observed that PopA-eYFP formed a single focus at the pole opposite to the stalk in  $\Delta popZ$  background (Fig. 4C). As *popZ* deletions lead to the mislocalization of many client proteins (50) and have pleiotropic effects on cell growth, we further explored PopA-eYFP localization in a PopZ overexpression strain (43). When PopZ is overproduced, the PopZ microdomain expands into a large volume (43), and we find PopA-eYFP fills the entire PopZ-rich region (Fig. 4D). Together, these results suggest that PopZ recruits PopA to the stalked pole. To determine whether PopZ interacts with PopA, we performed a BacTH assay by expressing PopA/PopZ and PopA<sub>R357G</sub>/PopZ in *E. coli*. We found that PopA interacts with PopZ, whereas no interaction was observed between PopA<sub>R357G</sub> and PopZ (Fig. 4B, right column). The difference between the capability of PopA and PopA<sub>R357G</sub> to interact with PopZ suggests that the interaction between PopA and PopZ is c-di-GMP dependent, which is consistent with the observation that PopA<sub>R357G</sub> is unable to localize to the stalked pole.

**PopA Performs Distinct Functions at the Two Opposing Cell Poles.** As the swarmer cell differentiates into a stalked cell, the composition of the pole bearing the flagellum changes dramatically. Morphologically, the flagellar filament and hook are ejected, pili are retracted, and the biogenesis of the stalk is initiated at the site vacated by the flagellum (Fig. 1A). This transition is accompanied by the assembly of a ClpXP proteolytic complex at the pole that specifically degrades the chemotaxis apparatus, the TacA protein (51), and the CtrA global regulatory transcription factor (52). The PopA protein at the stalked pole functions as a ClpXP adapter protein for the targeted degradation of CtrA (24). We have shown here that PopA exists as a dimer in the presence of c-di-GMP at the stalked pole. However, when PopA localizes to the flagella-bearing swarmer pole that lacks c-di-GMP, it does so as a monomer.

To explore the function of PopA monomers at the swarmer pole, we identified proteins that interact with PopA through BacTH screening and coimmunoprecipitation of (3xFLAG-tag)-PopA (Materials and Methods). In addition to the previously known interaction partners at the stalked pole (CtrA, ClpX, RcdA), we identified four interaction partners of PopA. These include FliG, FliM, and FliN [all three are flagellum switch complex proteins (53–56)] and CCNA\_01529 (hereafter referred to as “SmrF” for “swarmer regulator of flagellum”), which is a small (122-residue)

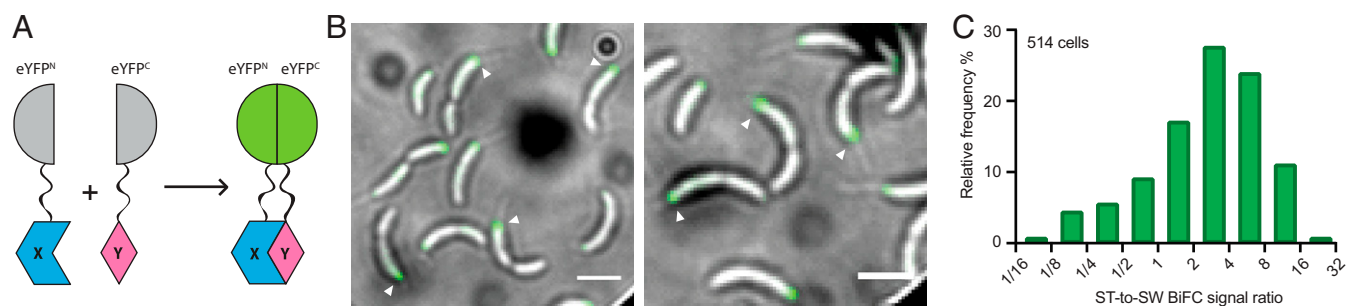


**Fig. 3.** PopA preferentially dimerizes at the stalked pole. (A) Schematic of a bimolecular fluorescence complementation assay (BiFC) to image protein-protein interactions. EYFP was split into N- and C-terminal fragments and fused to the C-terminal of proteins X and Y. Association between X and Y brings the two eYFP fragments into proximity, allowing the chromophore to mature and become fluorescent. (B) PopA BiFC signals. To assess oligomerization, both X and Y were PopA. PopA-eYFP<sup>N</sup> and PopA-eYFP<sup>C</sup> constructs were expressed from the *xyl* and *van* promoters, respectively, on the chromosome in a  $\Delta popA$  strain. Cells were induced with 0.03% xylose and 0.5 mM vanillate for 2 h before imaging. The white arrowheads indicate the stalked poles, and two field of views are shown. (Scale bars: 2  $\mu$ m.) (C) Log-frequency plot of the ratio of BiFC intensity between stalked and swarmer poles calculated from 514 predivisional cells that contained at least one fluorescent focus. Only 19.5% of the population had a brighter swarmer pole BiFC signal.

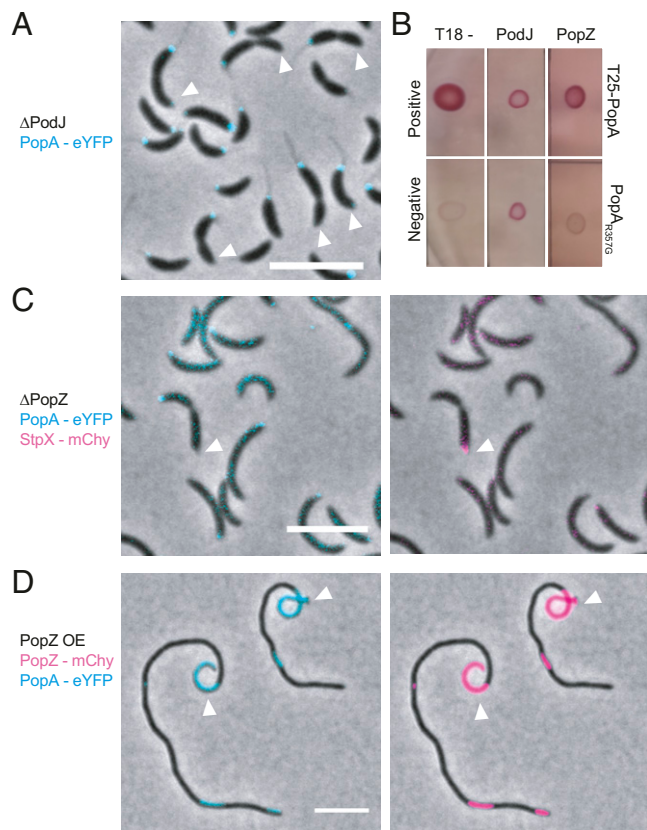


**Fig. 4.** PodJ and PopZ both regulate PopA localization. (A) PopA-eYFP was expressed from the native locus in a  $\Delta podJ$  strain. The white arrowheads indicate the swarmer poles with missing PopA-eYFP foci. From 543 predivisional cells, 80% cells had single foci at the stalked pole, while 18% exhibit bipolar foci. (Scale bars: 2  $\mu$ m.) (B) BacTH assays indicate positive PopA-PodJ and PopA<sub>R357G</sub>-PodJ interactions in vivo; positive PopA-PopZ interactions and the absence of interaction between PopA<sub>R357G</sub> and PopZ in vivo. (C) PopA-eYFP was expressed from the native locus in a  $\Delta popZ$  strain and the stalked-pole marker protein StpX was fused to a mCherry fluorescent protein. The white arrowheads indicate the stalked poles with missing PopA-eYFP foci. From 248 predivisional cells, 87% cells had single foci at the swarmer pole, while only 12% exhibit bipolar foci. (D) PopA-eYFP was expressed from the native locus and PopZ-mCherry was expressed from a high copy replicating plasmid. (Scale bars: 2  $\mu$ m.) Among 47 mixed-population cells, 83% of them showed more than one expanded PopZ region (magenta), in which PopA and PopZ always colocalize.

protein comprising a single FlaG-like domain (Pfam database) with unknown function. Notably, PopA interactions with these four proteins are *c*-di-GMP independent as the PopA<sub>R357G</sub> mutant bound effectively to these four proteins (Fig. 5A), consistent with the observation that the flagellated pole of the swarmer cell is devoid of *c*-di-GMP (29). In addition, the SmrF protein showed weak interaction with FliG and FliN and a lack of interaction with FliM (Fig. 5A).

**PopA Recruits SmrF to Regulate Flagellar Assembly.** While the function of the FlaG-like proteins remains elusive, the gene is always present in proximity to genes encoding flagellar assembly proteins (57–59) or flagellin (59, 60), suggesting a function related to the flagellum. In *Caulobacter*, *smrF* lies within the same operon, and immediately downstream of the flagellin encoding gene, *fljK* (61, 62), suggesting that its function might be related to flagella biogenesis. FljK is the major flagellin forming the majority of *Caulobacter* flagella filament, which is composed of six flagellin proteins in total (63, 64).

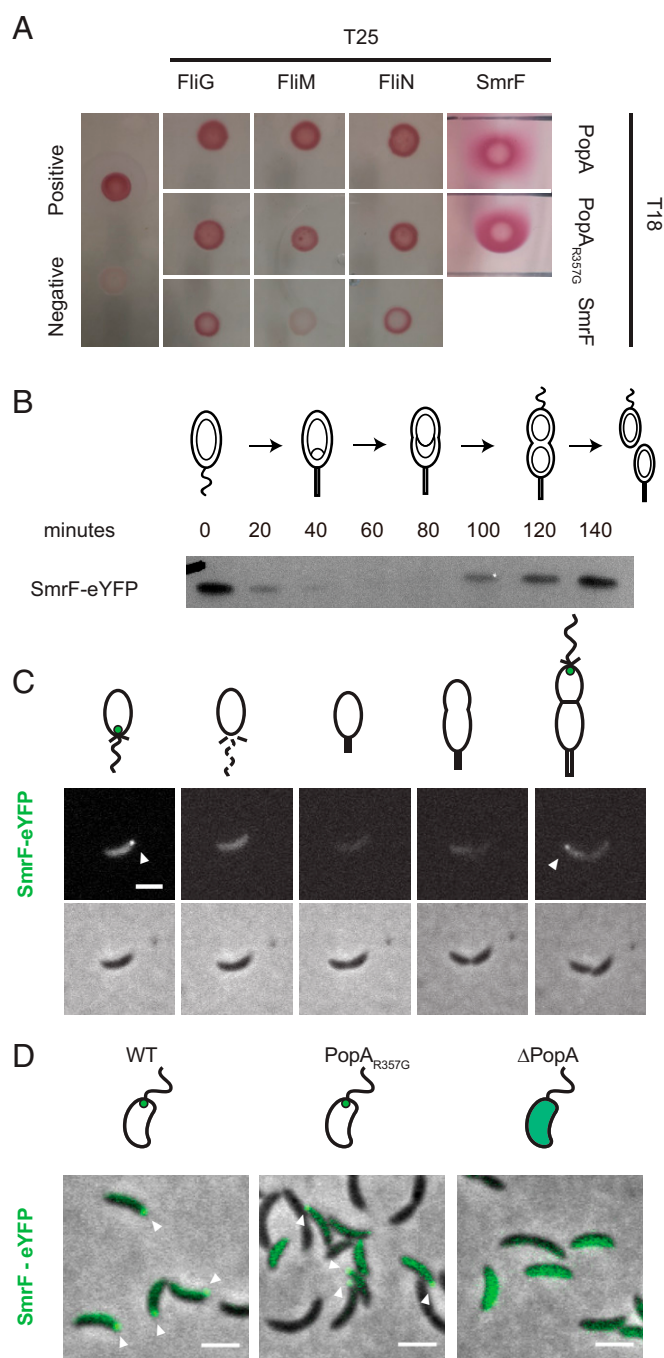


**Fig. 5.** PopA recruits SmrF to the swarmer pole. (A) BacTH assays indicate positive interactions between PopA and four proteins FliG, FliM, FliN, and SmrF in vivo, all of which were independent of *c*-di-GMP. Weak association was observed for SmrF-FliG and SmrF-FliN. (B) SmrF is cell cycle regulated. Using immunoblots with anti-eYFP antibody, we determined the relative presence of SmrF-eYFP through the cell cycle starting from swarmer cells. SmrF-eYFP construct was the only copy in the cell and was expressed from the native promoter. The accumulation of SmrF starts in the late predivisional cell, coincidental with flagellin synthesis (61). (C) Time-lapse microscopy analyses every 30 min show SmrF-eYFP accumulated at the new cell pole (swarmer pole) during the cell cycle. The white arrows indicate the swarmer poles. (Scale bars: 2  $\mu$ m.) (D) SmrF localization to the new pole requires PopA. Fluorescence images of SmrF-eYFP in WT, PopA<sub>R357G</sub>, and  $\Delta PopA$  strains. In all strains, the chromosomal *smrF* locus was replaced with *smrF-eYFP*. The white arrowheads indicate the swarmer poles. (Scale bars: 2  $\mu$ m.) For over 250 synchronized swarmer cells, over 95% of the WT and PopA<sub>R357G</sub> have a single polar focus of SmrF-eYFP, which were completely lost in  $\Delta PopA$  strains.

Construction of fusions of SmrF to eYFP allowed us to visualize the dynamic subcellular localization of SmrF during the cell cycle, where its abundance matches that of flagellar biosynthesis (Fig. 5B). Fluorescence imaging revealed that SmrF-eYFP only appeared at the flagellar pole in late predivisional cells, and the nascent daughter swarmer cells (Fig. 5C). In a strain bearing a PopA mutant (PopA<sub>R357G</sub>) unable to bind to c-di-GMP, SmrF-eYFP retained the ability to localize to the flagellar cell pole (Fig. 5D, Middle). SmrF-eYFP was present as a diffuse signal in a  $\Delta popA$  strain, suggesting a direct or indirect interaction with PopA (Fig. 5D, Bottom). Using microscale thermophoresis (MST), we measured the  $K_d$  of PopA-SmrF and PopA<sub>R357G</sub>-SmrF binding to be  $5.6 \pm 0.54$  and  $5.1 \pm 0.72$   $\mu$ M, respectively (SI Appendix, Fig. S4). Our results suggest that PopA directly recruits SmrF to the swarmer pole.

The SmrF protein is degraded during the swarmer-to-stalked cell transition, coincident with cell cycle-controlled proteolysis of the CtrA master regulator (16) (SI Appendix, Fig. S5A). To determine the factors that affect SmrF proteolysis, we constitutively expressed SmrF-eYFP from P<sub>xy1X</sub> promoter (65) in merodiploid strains containing the WT *smrF* gene. We measured the degradation of SmrF-eYFP in a  $\Delta popA$  strain, and in ClpX and ClpP depletion strains. We observed loss of proteolysis in all of these strains (SI Appendix, Fig. S5B), suggesting that SmrF degradation is performed by the ClpXP system using PopA as an adaptor, as is the case for CtrA proteolysis (16, 21, 24). Thus, the cell cycle regulation of SmrF is maintained by the same proteolytic system that controls the critical regulatory proteins PdeA, TacA, and CtrA (24). During the swarmer-to-stalked transition, cells begin to synthesize c-di-GMP rapidly reaching peak levels in the stalked cells (29, 30). Increasing the amount of c-di-GMP allows PopA to dimerize and turn on its function as the proteolysis adaptor for ClpXP and the degradation of both CtrA and SmrF commence following the swarmer-to-stalked cell transition (21–24) (SI Appendix, Fig. S5A).

Although a *smrF* deletion strain or a SmrF overexpression strain did not exhibit viability defects in rich PYE or minimal M2G media (SI Appendix, Fig. S6A), and both strains exhibited normal sized swarm colonies on rich or minimal soft agar plates (SI Appendix, Fig. S6B), swarmer cells of a *smrF* deletion strain had longer flagella, while overproduction of SmrF protein produced shorter flagella compared to WT (Fig. 6A and B). While the length of the flagellum could be controlled by an increase in swarmer cell life span before it differentiates in to stalked cell, the deletion of *smrF* does not alter the swarmer cell life span as shown in SI Appendix, Fig. S7.

If the time of flagellum construction is constant, either an increase in flagellin expression or flagellin secretion, or both, can result in longer flagella. Accordingly, we asked whether SmrF serves as a regulatory protein for flagellin expression. However, SmrF and the FlaG superfamily proteins in general, are not known as DNA or RNA binding proteins. We entered the SmrF sequence into DRNAPred to predict its DNA binding probability (66). While the program indicated that SmrF is not a DNA-binding protein, it might interact with RNA. It has been shown that *Caulobacter* synthesizes flagellin mRNAs in predivisional cells (67). We used fluorescently labeled fluorescence in situ hybridization (FISH) probes to investigate the spatial distribution of flagellin mRNAs and observed only diffuse fluorescent signal in the cytosol away from the polar regions (Fig. 6C), implying that flagellin mRNAs do not accumulate at the pole where SmrF forms foci. The absence of colocalization of SmrF and flagellin mRNA implies that they do not strongly interact. In addition, the PopZ polar microdomain excludes the ribosome translation machinery (50). Hence, it is unlikely that SmrF regulates flagellin on either the transcriptional or translational level.

As PopA interacts with the flagellar motor switch proteins FliG, FliM, FliN, and SmrF is targeted to the pole through direct binding to PopA, PopA likely recruits SmrF into the vicinity of

the flagellum basal body in order to perform its regulatory role. In the discussion below, we consider the possibility that at the swarmer pole the PopA/SmrF complexes are involved in flagellin secretion by docking onto the flagellum basal body.

## Discussion

We have demonstrated that PopA employs c-di-GMP concentration differences as spatial cues to perform distinct roles at the opposing cell poles by adopting different oligomeric states. PopA complexes at the two cell poles appear to be intrinsically different: Stalked pole localization of dimeric PopA is c-di-GMP dependent, while swarmer pole localization of monomeric PopA is c-di-GMP independent. PopA localized at the stalked pole in the presence of c-di-GMP functions as a ClpXP protease adaptor enabling CtrA degradation, while PopA at the swarmer pole appears to regulate the final step in flagella biogenesis, filament assembly. In each case, PopA recognizes different proteins at each pole, and is an accessory factor that contributes to the function of a complex biomolecular machinery (Fig. 7).

*Caulobacter* employs multiple proteins to synthesize and hydrolyze c-di-GMP (30). By positioning pairs of antagonistic enzymes to the opposing poles, cells acquire asymmetrically distributed c-di-GMP concentrations in the polar regions: The diguanylate cyclase PleD is localized and activated at the stalked pole (27) while the phosphodiesterase PdeA is sequestered to the swarmer pole (28). We have provided evidence that the high local concentration of c-di-GMP at the stalked pole drives PopA to adopt a dimeric form and that the low local concentration of c-di-GMP at the swarmer pole allows PopA to remain monomeric. c-di-GMP can be detected in the cytosol outside the polar regions due to the facile diffusion of this small molecule (29), which appears to be sufficient to keep PopA in dimeric form (Fig. 1A).

Binding assays using BacTH system revealed that PopA self-association is c-di-GMP dependent. PopA<sub>R357G</sub>, which is unable to bind c-di-GMP, was unable to form dimers in an *E. coli* heterologous system (Fig. 1C). Diffusion analysis further revealed that the presence of c-di-GMP changes the diffusive properties of PopA (Fig. 2). In the absence of c-di-GMP, PopA diffuses in a complex half the size compared to that when c-di-GMP is present, supporting the hypothesis that PopA exists in a dimeric form at one pole and in a monomeric form at the other. BiFC assays directly demonstrated PopA dimerization and its preferential dimerization at the stalked pole, which is the site of c-di-GMP synthesis (Fig. 3).

The intrinsically disordered protein PopZ is a polar organizing protein that accumulates at the two cell poles and form space filling microdomains of 100 to 200 nm (43–47). The microdomains selectively recruit and concentrate signaling proteins including PopA (Figs. 1 and 4). The primary enzymes that synthesize and hydrolyze c-di-GMP are differentially deployed also at the cell poles (27, 28) and have been shown to interact with PopZ (45). The two catalytic reaction centers create an environment for PopA such that the local concentration of c-di-GMP is higher at the stalked than at the swarmer pole. The limited availability of c-di-GMP at the swarmer pole prevents PopA from dimerizing.

Upon dimerization, PopA exposes a different surface to the cytosol allowing the protein to interact with a new set of binding partners. The distinct behavior of PopA polar sequestration at the two cell poles implies that PopA might be recruited by different proteins. In previous deletion studies, PopA stalked pole localization is PopZ dependent while swarmer pole localization is PodJ dependent (22). We showed that PopA, indeed, interacts with both PodJ and PopZ. Moreover, the interaction between PopA and PodJ at the swarmer pole is c-di-GMP independent and that PopA and PopZ interaction at the stalked pole requires c-di-GMP (Fig. 4).

Changes in c-di-GMP concentration as a function of the cell cycle not only triggers the switch of PopA between monomeric and dimeric form but also activates signaling pathways important for the transition from swarmer-to-stalked cells (30). The

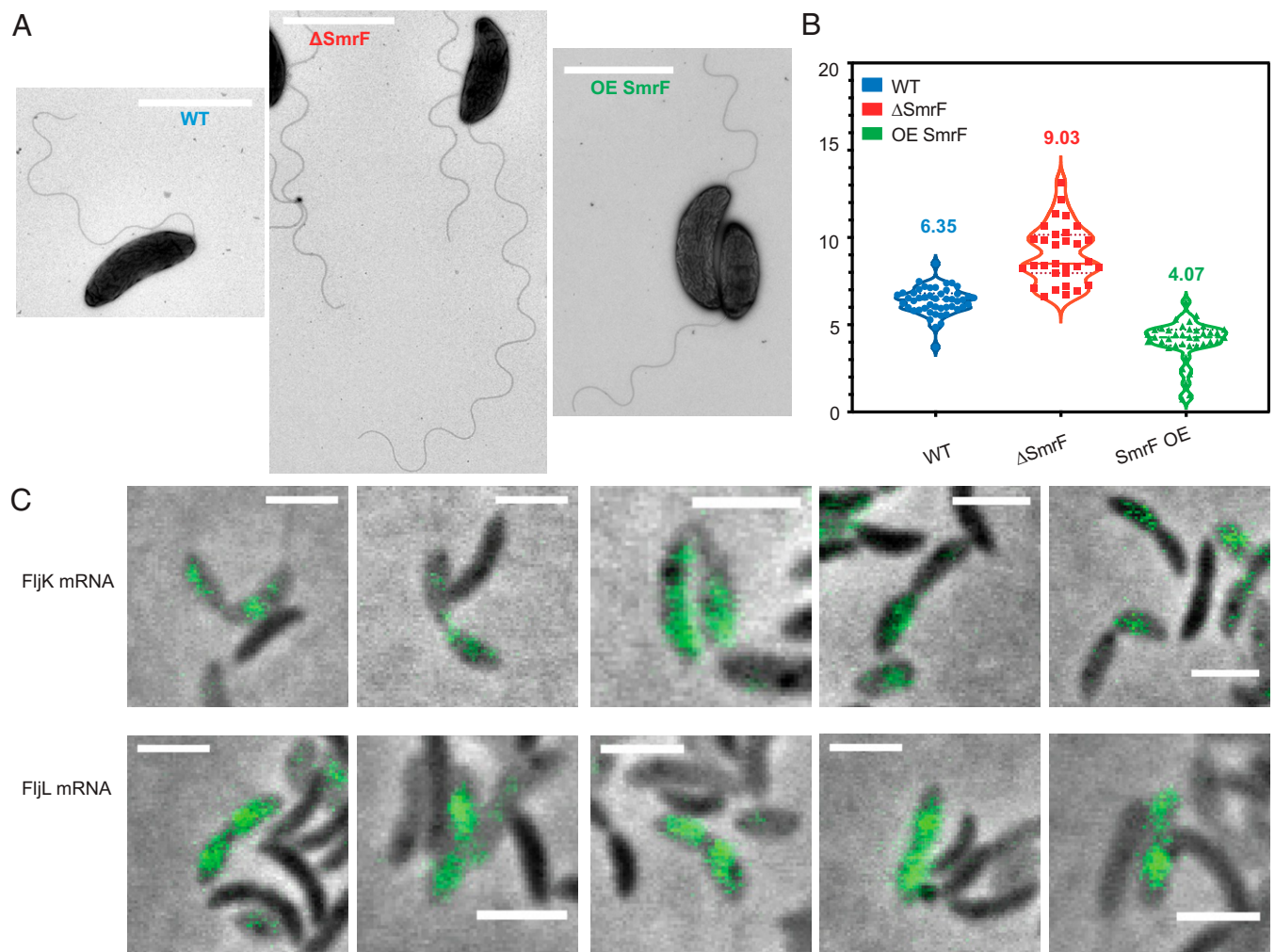


**Fig. 6.** SmrF negatively regulates flagellar length and interacts with flagellar proteins. (A) Transmission electron micrographs of the flagella in wild-type (WT) (Left),  $\Delta smrF$ , and SmrF overexpression cells. (Scale bars: 2  $\mu\text{m}$ .) (B) Deletion of *smrF* causes an increased flagellar-length phenotype, while overexpression of *smrF* yields shortened flagella. Flagellar length was calculated from over 30 cells for each strain using ImageJ. (C) mRNA of flagellin FliJ and FliL do not accumulate at the swarmer cell pole. The figure shows multiple imaging fields where the FliJ and FliL mRNA are imaged by FISH. (Scale bars: 2  $\mu\text{m}$ .)

concentration of c-di-GMP peaks in the stalked cells and is reduced by hydrolysis in swarmer cells (29). Previously, only the stalked pole function of PopA was known. Here, we identified a protein, SmrF, that is sequestered to the swarmer pole by PopA. The deletion and overexpression of the *smrF* gene did not show any viability or motility defects, but cells lacking *smrF* construct exceptionally long flagella filaments. The *smrF* gene belongs to the *flaG* super family, which is prevalent among the alphaproteobacteria (*Rhizobium*, *Nitrobacter*) and is found in many other proteobacteria species (*Rhodocyclales*, *Pseudomonas*, *Desulfobibrionales*, *Campylobacterales*). Nonmotile, flagellum-less bacteria such as *Klebsiella pneumoniae*, *Yersinia pestis*, *Streptococcus*, and *Shigella* do not have genes that belong to the *flaG* superfamily. While the function of the FlaG proteins remains elusive and is unlikely to be a flagellin subunit, the gene is always present in proximity to flagellin genes, suggesting a related function to filament assembly. In *Campylobacter jejuni*, a deletion of *flaG* yields extremely long flagella (58), as is the case in *Pseudomonas fluorescens*, bearing a mutation in *flag* (59), and in *Vibrio anguillarum*, bearing an insertion in *flaG* open reading frame (60).

The spatial localization of FlaG proteins in other species is unknown. In *Caulobacter*, the cytosolic FlaG ortholog, SmrF, is recruited to the swarmer pole by PopA (Fig. 5D). We provide

evidence that SmrF does not change the swarmer cell life span or motility and is unlikely to regulate the transcription of flagellin genes. As is well known, *Caulobacter* tethers the origin of its single circular chromosome to the pole, and each gene locus has a defined subcellular address (68). The locations of flagellin genes are not near either pole (68); hence SmrF cannot colocalize with flagellin gene loci. In addition, a FISH experiment (Fig. 6C) demonstrated that flagellin mRNAs distribute evenly throughout swarmer cells. Finally, as PopA also interacts with all three components of the flagellum switch complex (Fig. 5A) that surrounds the secretion pore, it is possible that PopA recruits SmrF to physically block the secretion of flagellin monomers. A definition of the underlying mechanism is a topic of ongoing research.

Here, we demonstrated that the asymmetric distribution of c-di-GMP in the predivisional cell translates into the formation of two distinct PopA oligomeric states, which in turn interact with two different cellular machineries, the ClpXP degradation machinery at the stalked pole and flagellum basal body at the swarmer pole (Fig. 7). During the swarmer-to-stalked transition, c-di-GMP synthesis triggers the dimerization of PopA and switches PopA function from flagellar regulation to proteolysis adaptor. The degradation of SmrF by the ClpXP ensues. Interestingly, SmrF overexpression does not lead to delayed CtrA degradation

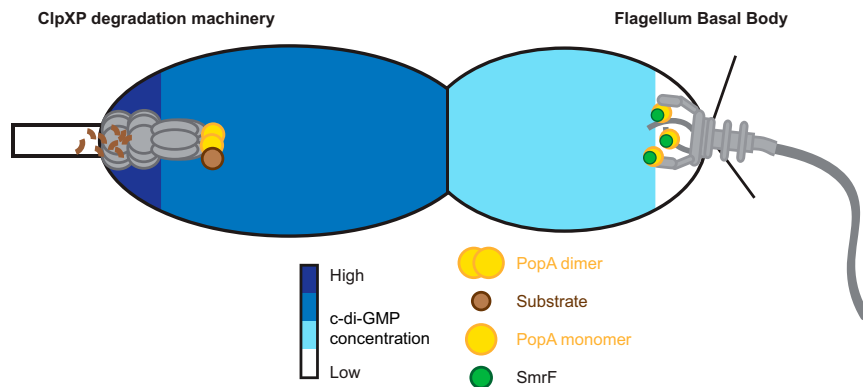


**Fig. 7.** PopA oligomerization senses local c-di-GMP concentration yielding different oligomeric states at two poles that perform distinct roles. PopA (yellow circles) translates the asymmetric subcellular distribution of c-di-GMP (blue) shown in Fig. 1 into the formation of two distinct oligomeric states. The dimeric form of PopA interacts with the ClpXP machinery at the stalked pole and facilitates CtrA degradation. The monomeric form of PopA accumulates near the flagellum basal body at the swarmer pole and recruits SmrF (green circles) to regulate flagellum synthesis.

(SI Appendix, Fig. S7), suggesting that SmrF does not compete with CtrA as a substrate of the ClpXP.

Studies have demonstrated that throughout evolution the availability of second messenger molecules can modulate protein activities (10, 69–71). Our analysis of PopA expands the repertoire of signaling schemes of second messenger sensing proteins by demonstrating how ligand availability can toggle distinct oligomeric states to achieve multiple functional states. Collectively, these studies of second messenger binding proteins suggest that second messenger molecules can provide spatial cues for proteins to adopt different forms and functions that enable asymmetric cell division.

## Materials and Methods

**Cell Preparation.** All *Caulobacter* strains used for imaging were grown in minimal media M2G at 28 °C and collected at midlog phase (72) onto 1.5% (wt/wt) agarose pads made with M2G. For single-molecule tracking experiments, cells were washed three times with fresh M2G. Synchronized swarmer cells were collected by density centrifugation using Percoll (73). Synchronized swarmer cells were recovered in M2G at 28 °C for 5 min before imaging or let grow for 30 min to reach stalked cell stage before imaging (73). For single-molecule tracking experiments, 100-nm fiducial markers (Molecular Probes; 540/560 carboxylate-modified FluoSpheres) at around 1 nM were added to the cells before imaging.

**Protein Purification.** His6-PopA, His6-PopA<sub>R357G</sub> were expressed from the pET28b vectors (21), and His6-SmrF was expressed from the pACYCDuet-1 vectors indicated in SI Appendix, Table S1. All proteins were purified using the following protocol adapted from Smith et al. (23). Proteins were expressed in *E. coli* BL21 cells (C2566H; NEB) grown to OD<sub>600</sub> of 0.4 at 37 °C in LB broth. The 0.4 mM isopropyl-β-D-thiogalactoside was used to induce protein expression overnight at 16 °C. Cells were harvested and the cell pellets were resuspended in lysis buffer (50 mM Tris-HCl, pH 8.2, 100 mM KCl, 1 mM MgCl<sub>2</sub>, 10% glycerol, 2 mM 2-mercaptoethanol) supplemented with protease inhibitors (Santa Cruz Biotechnology) and benzonase nuclease (Sigma). Cells were lysed using five passes through an EmulsiFlex (Avestin). Lysates were treated by centrifugation at 4 °C and incubated with Ni-NTA agarose resin for 1 h at 4 °C after adding 20 mM imidazole. We used 5 mL of NTA slurry/1 L of initial cell culture when purifying PopA, and 1 mL of NTA slurry/1 L of initial cell culture when purifying SmrF. The protein bound Ni-NTA resin was washed five times at 4 °C. The proteins were eluted with 10 mL of lysis buffer/1 L of initial culture supplemented with 300 mM imidazole using Poly-Prep chromatography columns (Bio-Rad). Ten millimolar EDTA was added to all eluted proteins before they were buffer exchanged into storage buffer, 25 mM Hepes-KOH, pH 8.0, 100 mM KCl, 5 mM MgCl<sub>2</sub>, 15 mM NaCl, 5% (vol/vol) glycerol, and 1 mM DTT, before freezing in liquid nitrogen and storage at –80 °C.

**Cross-Linking Assay.** We cross-linked PopA by adapting a protocol that was used to study a paralogous protein PleD (74). The purified PopA (at 0.1, 0.25, 0.5, and 1 mg/mL concentration) was incubated with or without 1 mM c-di-

GMP at 4 °C overnight. A water-soluble cross-linker BS3 (Abcam) was added at 2.5 mM final concentration for 30 min at room temperature to cross-link the protein. The reaction was quenched by adding Tris-HCl, pH 8.0, 50 mM final concentration. After separation on 4–15% precast polyacrylamide gel (Bio-Rad) and transfer to a PVDF membrane (GE Healthcare), PopA monomeric and dimeric forms were detected by staining with a polyclonal anti-PopA antibody (Josman). Secondary goat-anti-rabbit immunoglobulin G with HRP (Abcam; ab205718) conjugation was used for visualization.

**MST Binding Assays.** PopA and PopA<sub>R357G</sub> were fluorescently labeled on lysine residues with *N*-hydroxysuccinimide functionalized Atto-488 (Sigma-Aldrich). The dye conjugate was dissolved in dry DMSO to make stock solution. The conjugation reaction was performed in the dark using 1.5 mg/mL protein and a threefold molar ratio of dye to protein at room temperature with gentle shaking for 15 min. Each protein was labeled with one to two dye molecules on average. Proteins were buffer exchanged into the same storage buffer through overnight dialysis to remove unlabeled dye molecules. The labeled proteins were diluted to 2 μM and flash frozen in liquid nitrogen and storage at –80 °C. Direct binding between fluorescently labeled PopA or PopA<sub>R357G</sub>, with c-di-GMP (Axxora), unlabeled PopA or PopA<sub>R357G</sub>, as well as SmrF was probed in twofold serial dilutions using MST (75) (NanoTemper Technologies) (75, 76).

All proteins used for MST were dialyzed into MST buffer (50 mM Tris-HCl, pH 8.0, 150 mM NaCl, 5 mM MgCl<sub>2</sub>, 1 mM DTT with 0.025% Tween 20) overnight. For each binding assay, a twofold serial dilution was made for each protein target and c-di-GMP in MST buffer. Fluorescently labeled PopA (or PopA<sub>R357G</sub>) was added at 25 nM, mixed, and incubated at room temperature for 15 min in the dark. The protein mixtures were then loaded into Standard Treated capillaries (NanoTemper). Binding was assessed using the following instrument setting: 80% blue LED power, 60% IR-laser power, 5-s initial measurement, 25-s IR heating period, and 5-s recovery. Binding data were fit using MO.Affinity Analysis (NanoTemper), and the binding curve plateau data were exported. Experimental replicates were averaged and fitted with Prism 7 (GraphPad) according to the law of mass action, as previously described (75):

$$\frac{BL}{B_0} = \frac{([L_0] + [B_0] + K_d) - \sqrt{([L_0] + [B_0] + K_d)^2 - 4 * [L_0] * [B_0]}}{2[B_0]}$$

In this equation, *BL* represents the concentration of protein complexes, *[B<sub>0</sub>]* represents total binding sites of the fluorescent ligand, *[L<sub>0</sub>]* represents the amount of added ligand, and *K<sub>d</sub>* represents the dissociation constant.

**BactH Assay.** Protein pairs were fused in frame to the C or N terminus of the T18 and T25 subunits of the adenylate cyclase. Paired constructs were expressed in the *E. coli* BTH101 cell line, which is depleted of any activity of adenylate cyclases. Cells were then plated on MacConkey agar. Magenta colonies indicate protein–protein interaction. We used the self-associating leucine zipper, T25-zip and T18-zip, as a positive control and T18 and T25 alone as a negative control (77).

**Transmission Electron Microscopy.** For flagellum visualization, cells were grown in M2G media to OD<sub>600</sub> of 0.5 with gentle shaking at 30 °C. Two

microliters of cell culture were applied to glow-discharged, carbon-coated copper grids (EMS, FCF300-Cu-25) and negatively stained with 0.5% (wt/vol) uranyl acetate. The grids were then washed three times before imaging. Centrifugation damages the flagellum integrity and must be avoided during preparation. Data were collected using a JEM1400, a JEOL 120-keV transmission electron microscope at various magnification settings. The length of flagellum was quantified by manually tracing the flagellum in ImageJ.

**Coimmunoprecipitation.** One liter of *Caulobacter* cells expressing PopA-3xFLAG and GapR-3xFLAG (nonpolar protein control) were cultured in M2G minimal media at 28 °C, and cells were harvested at midlog phase. All following steps were conducted at 4 °C. The pelleted cells were then washed three times with IP buffer (20 mM Hepes, pH 7.5, 150 mM NaCl, 10% glycerol, protease inhibitor, and benzonase nuclease) to remove remaining growth media. The cells were resuspended in 20 mL of IP buffer, and DSP (Lomant's reagent, Thermo Fisher, dissolved in DMSO) was added to a final concentration of 2 mM. The mixture was incubated for 2 h with nutation. The cross-linking reaction was terminated by adding Tris-Cl, pH 7.5, at a final concentration of 20 mM and incubated for 15 min. The cells were then lysed using an EmulsiFlex (Avestin) until lysates cleared. Cellular debris was removed from the lysates by centrifugation and the lysates were incubated with anti-FLAG magnetic beads (Sigma) overnight with nutation. The next morning, the magnetic beads were washed five times with 10 mL IP buffer each time. Finally, proteins were eluted by 200  $\mu$ L of 0.1 mg/mL 3xFLAG peptide (Sigma). The protein mixture was denatured and run on SDS polyacrylamide gel before being sent to the Stanford University Mass Spectrometry facility for protein identification.

**FISH.** We adapted a smFISH protocol to visualize flagellin mRNA in *Caulobacter* cells (78). FISH probes targeting flagellin sequences were designed using Stellaris Probe Designer and ordered from the Stanford PAN facility. FijK and FijL were targeted by 13 and 11 probes, respectively. Probes were 20 nucleotides long with GC content ranging from 40 to 55% with 3' amino modifier C7. Twenty-five nanomoles of each probe were synthesized and dissolved in water to a final concentration of 100  $\mu$ M.

We combined equal volumes of each probe for labeling and added about 1/9 of the reaction volume of 1 M sodium bicarbonate (pH 8.5) to reach a final concentration of 0.1 M sodium bicarbonate. The 20  $\mu$ g/ $\mu$ L Alexa 568 succinimidyl ester dissolved in DMSO was mixed with probe mixture. The reaction mixture was incubated on a nutator at 37 °C in the dark overnight. To terminate the labeling reaction, 1/9 reaction volumes of 3 M sodium acetate (pH 5.2) was added to a final concentration of 0.3 M. The probes were purified from unconjugated free dye with a PCR cleanup kit. All probes were labeled with over 85% efficiency.

We collected 1 mL of *Caulobacter* cells grown into midlog phase in M2G and resuspended into 1 mL of 3.7% formaldehyde in PBS. The cell mixture was incubated at room temperature for 15 min and washed twice with 1x PBS. The cells were resuspended in 300  $\mu$ L of ddH<sub>2</sub>O and 1  $\mu$ L of 50  $\mu$ g/mL lysozyme in GTE buffer (50 mM glucose, 25 mM Tris, 10 mM EDTA, pH 7.5). Cells were permeabilized in this reaction mix for 4 min.

The supernatant was then removed after centrifugation, and 1 mL of 40% wash solution (10% formamide in 3x saline sodium citrate) was added to the cell pellet for 3 min and let stand. In a different tube, we added 50  $\mu$ L of hybridization solution (10% dextran sulfate, 1 mg/mL *E. coli* tRNA, 0.2 mg/mL BSA, 2 mM vanadyl ribonucleoside complexes, 10% formamide in 2x saline sodium citrate) and 1  $\mu$ L of 10x diluted probe solution (15 nM final concentration). The cell mixture was centrifuged, the supernatant was removed, and finally the pellet was resuspended in hybridization solution containing probes. The hybridization reaction was left at 30 °C overnight.

The next day, cells were washed three times with 200  $\mu$ L of wash solution, and each time after mixing well, the tube was incubated at 30 °C for 30 min. Finally, cells were suspended into 10  $\mu$ L of 2x saline sodium citrate for imaging.

**Single-Molecule Imaging.** *Caulobacter* cells are around 0.5- $\mu$ m diameter by 2- to 4- $\mu$ m long, which is on the same order of magnitude as the diffraction

limit (~250 nm). To accurately track movements of single proteins in live cells, we use superlocalization to pinpoint the location of single molecules where photobleaching was used to reduce the emitting concentration (44, 48, 79). Live cells were immobilized on agarose pad that was bleached overnight before the experiment. Single-molecule imaging experiments were performed on a custom epifluorescence microscope (Nikon; Diaphot 200) equipped with a Si EMCCD camera (Andor; iXon DU-897) and a high numerical aperture (N.A.) oil-immersion objective (Olympus; UPlanSapo, 100x/1.4 N.A.). Molecules were excited with either 514-nm, 1-W continuous-wave laser or 642-nm, 1-W continuous-wave laser (MPB Communications) and photoactivated by a 405-nm Obis laser at 0.8 kW/cm<sup>2</sup>, 0.65 kW/cm<sup>2</sup>, and 0.1 to 1 W/cm<sup>2</sup>, respectively. The emission from fluorescent molecules was collected through a four-pass dichroic mirror (Semrock; Di01-R405/488/561/635) and filtered by a 514-nm long-pass filter (Semrock; LP02-514RE), a 560-nm dichroic beam splitter (Semrock; FF560-FD101), a 561-nm notch filter (Semrock; NF03-561E), and a bandpass filter (Semrock; FF01-532/610) as previously described (48, 79).

**Single-Molecule Localization and Single-Particle Tracking.** We wrote a custom MATLAB script to remove background using temporal medium filtering and processed the single-molecule images for two-dimensional (2D) Gaussian fitting by ThunderSTORM (ImageJ) (80). We used the local maximum algorithm to estimate localization of molecules with a 2.2xstd peak intensity threshold and eight-neighborhood connectivity. A 3-pixel fitting radius was used to fit the point spread function using weighted least-square method. The localization precision was approximately 25 nm for PopA-eYFP as estimated by the SD of successive localizations of stationary molecules in 20 ms frames. Custom MATLAB code was used to extract trajectories of single proteins whose calculated positions show up in contiguous frames and in the same cells as performed previously (44). Within any frame, if one cell contained more than one localization, the case was discarded to avoid categorization errors. All the localizations were then output into custom MATLAB scripts to generate cellular trajectories by connecting localizations from consecutive frames. Tracks that were at least three steps (four frames) were collected and 20 bootstrapped samples were taken (80% of total trajectories) for the MSD analysis. To minimize the confounding effect of cellular confinement, diffusion coefficients were calculated from the first two time lags of the ensemble-averaged MSDs of each bootstrapped sample by fitting with a modification of the standard equation for Brownian motion that takes into account dynamic and static errors (81):

$$\text{MSD}(\tau) = 4D\left(\tau - \frac{\Delta t}{3}\right) + 2\sigma_x^2 + 2\sigma_y^2.$$

$\Delta t$  represents the frame integration time, and  $\tau$  lag time. The diffusion coefficient  $D$ , and localization error in  $x$  and  $y$ ,  $\sigma_x$ ,  $\sigma_y$ , are free parameters determined by least-squares fit.

**Data Availability.** All figures and other data have been deposited in the publicly available Stanford Digital Repository (<https://purl.stanford.edu/gx629ky7112>).

**ACKNOWLEDGMENTS.** We thank Urs Jenal for providing plasmids and strains. We acknowledge Annina Schalch-Moser from the Jenal laboratory for her thesis work on PopA, which we accessed after the completion of the experiments reported in this paper. We thank John Perrino and Jonathan Mulholland (Cell Science Imaging Facility, Stanford University) for technical guidance on the transmission electron microscopy. We thank Lexy von Diezmann, Keren Lasker, Peter Dahlberg, Eduardus de Koning, and all members of the L.S. laboratory and the W.E.M. laboratory for helpful comments and discussion. This work was supported in part by National Institute of General Medical Sciences Grants R35GM118067 (to W.E.M.) and R35GM118071 (to L.S.). J.W. is a Mona M. Burgess Stanford Bio-X Fellow and was supported by Stanford Center for Molecular Analysis and Design during the early stage of this project. L.S. is a Chan Zuckerberg Biohub Investigator. W.E.M. is a Chan Zuckerberg Biohub Intercampus Research Award Collaborator.

1. Y. M. Yamashita, M. T. Fuller, Asymmetric centrosome behavior and the mechanisms of stem cell division. *J. Cell Biol.* **180**, 261–266 (2008).
2. M. Inaba, Y. M. Yamashita, Asymmetric stem cell division: Precision for robustness. *Cell Stem Cell* **11**, 461–469 (2012).
3. L. Shapiro, H. H. McAdams, R. Losick, Generating and exploiting polarity in bacteria. *Science* **298**, 1942–1946 (2002).
4. G. R. Bowman, A. I. Lyuksyutova, L. Shapiro, Bacterial polarity. *Curr. Opin. Cell Biol.* **23**, 71–77 (2011).
5. C. Jacobs, I. J. Domian, J. R. Maddock, L. Shapiro, Cell cycle-dependent polar localization of an essential bacterial histidine kinase that controls DNA replication and cell division. *Cell* **97**, 111–120 (1999).
6. S. G. Martin, M. Berthelot-Grosjean, Polar gradients of the DYRK-family kinase Pom1 couple cell length with the cell cycle. *Nature* **459**, 852–856 (2009).
7. A. Treuner-Lange, L. Sogaard-Andersen, Regulation of cell polarity in bacteria. *J. Cell Biol.* **206**, 7–17 (2014).
8. C. Jacobs, N. Ausmees, S. J. Cordwell, L. Shapiro, M. T. Laub, Functions of the CckA histidine kinase in *Caulobacter* cell cycle control. *Mol. Microbiol.* **47**, 1279–1290 (2003).
9. J. Mignolet et al., Functional dichotomy and distinct nosanose assemblies of a cell cycle-controlled bipolar zinc-finger regulator. *eLife* **5**, e18647 (2016).
10. T. H. Mann, W. Seth Childers, J. A. Blair, M. R. Eckart, L. Shapiro, A cell cycle kinase with tandem sensory PAS domains integrates cell fate cues. *Nat. Commun.* **7**, 11454 (2016).

11. B. M. Gumbiner, Regulation of cadherin-mediated adhesion in morphogenesis. *Nat. Rev. Mol. Cell Biol.* **6**, 622–634 (2005).
12. M. Ozawa, H. Baribault, R. Kemler, The cytoplasmic domain of the cell adhesion molecule uvomorulin associates with three independent proteins structurally related in different species. *EMBO J.* **8**, 1711–1717 (1989).
13. C. Mosimann, G. Hausmann, K. Basler, Beta-catenin hits chromatin: Regulation of Wnt target gene activation. *Nat. Rev. Mol. Cell Biol.* **10**, 276–286 (2009).
14. L. Shapiro, H. H. McAdams, R. Losick, Why and how bacteria localize proteins. *Science* **326**, 1225–1228 (2009).
15. P. D. Curtis, Y. V. Brun, Getting in the loop: Regulation of development in *Caulobacter crescentus*. *Microbiol. Mol. Biol. Rev.* **74**, 13–41 (2010).
16. I. J. Domian, K. C. Quon, L. Shapiro, Cell type-specific phosphorylation and proteolysis of a transcriptional regulator controls the G1-to-S transition in a bacterial cell cycle. *Cell* **90**, 415–424 (1997).
17. M. T. Laub, S. L. Chen, L. Shapiro, H. H. McAdams, Genes directly controlled by CtrA, a master regulator of the *Caulobacter* cell cycle. *Proc. Natl. Acad. Sci. U.S.A.* **99**, 4632–4637 (2002).
18. K. C. Quon, G. T. Marczyński, L. Shapiro, Cell cycle control by an essential bacterial two-component signal transduction protein. *Cell* **84**, 83–93 (1996).
19. A. A. Iniesta, L. Shapiro, A bacterial control circuit integrates polar localization and proteolysis of key regulatory proteins with a phospho-signaling cascade. *Proc. Natl. Acad. Sci. U.S.A.* **105**, 16602–16607 (2008).
20. K. R. Ryan, E. M. Judd, L. Shapiro, The CtrA response regulator essential for *Caulobacter crescentus* cell-cycle progression requires a bipartite degradation signal for temporally controlled proteolysis. *J. Mol. Biol.* **324**, 443–455 (2002).
21. A. Duerig *et al.*, Second messenger-mediated spatiotemporal control of protein degradation regulates bacterial cell cycle progression. *Genes Dev.* **23**, 93–104 (2009).
22. S. Ozaki *et al.*, Activation and polar sequestration of PopA, a c-di-GMP effector protein involved in *Caulobacter crescentus* cell cycle control. *Mol. Microbiol.* **94**, 580–594 (2014).
23. S. C. Smith *et al.*, Cell cycle-dependent adaptor complex for ClpXP-mediated proteolysis directly integrates phosphorylation and second messenger signals. *Proc. Natl. Acad. Sci. U.S.A.* **111**, 14229–14234 (2014).
24. K. K. Joshi, M. Bergé, S. K. Radhakrishnan, P. H. Viollier, P. Chien, An adaptor hierarchy regulates proteolysis during a bacterial cell cycle. *Cell* **163**, 419–431 (2015).
25. A. A. Iniesta, P. T. McGrath, A. Reisenauer, H. H. McAdams, L. Shapiro, A phospho-signaling pathway controls the localization and activity of a protease complex critical for bacterial cell cycle progression. *Proc. Natl. Acad. Sci. U.S.A.* **103**, 10935–10940 (2006).
26. P. T. McGrath, A. A. Iniesta, K. R. Ryan, L. Shapiro, H. H. McAdams, A dynamically localized protease complex and a polar specificity factor control a cell cycle master regulator. *Cell* **124**, 535–547 (2006).
27. R. Paul *et al.*, Cell cycle-dependent dynamic localization of a bacterial response regulator with a novel di-guanylate cyclase output domain. *Genes Dev.* **18**, 715–727 (2004).
28. S. Abel *et al.*, Regulatory cohesion of cell cycle and cell differentiation through interlinked phosphorylation and second messenger networks. *Mol. Cell* **43**, 550–560 (2011).
29. M. Christen *et al.*, Asymmetrical distribution of the second messenger c-di-GMP upon bacterial cell division. *Science* **328**, 1295–1297 (2010).
30. S. Abel *et al.*, Bi-modal distribution of the second messenger c-di-GMP controls cell fate and asymmetry during the *Caulobacter* cell cycle. *PLoS Genet.* **9**, e1003744 (2013).
31. A. Reinders *et al.*, Expression and genetic activation of cyclic Di-GMP-specific phosphodiesterases in *Escherichia coli*. *J. Bacteriol.* **198**, 448–462 (2015).
32. A. Schachl-Moser, “Insights into the activation mechanism of PopA, a cyclic di-GMP effector protein involved in cell cycle and development of *Caulobacter crescentus*,” PhD thesis, University of Basel, Basel, Switzerland (2012).
33. H. C. Berg, *Random Walks in Biology* (Princeton University Press, 1993).
34. L. Möckl, W. E. Moerner, Super-resolution microscopy with single molecules in Biology and beyond—essentials, current trends, and future challenges. *J. Am. Chem. Soc.* **142**, 17828–17844 (2020).
35. H. Shen *et al.*, Single particle tracking: From theory to biophysical applications. *Chem. Rev.* **117**, 7331–7376 (2017).
36. A. Einstein, Über die von der molekularkinetischen Theorie der Wärme geforderte Bewegung von in ruhenden Flüssigkeiten suspendierten Teilchen. *Ann. Phys.* **322**, 549–560 (1905).
37. A. Einstein, *Investigations on the Theory of the Brownian Movement* (Dover Publications, 1956).
38. T. K. Kerppola, Design and implementation of bimolecular fluorescence complementation (BiFC) assays for the visualization of protein interactions in living cells. *Nat. Protoc.* **1**, 1278–1286 (2006).
39. R. H. Rose, S. J. Briddon, N. D. Holliday, Bimolecular fluorescence complementation: Lighting up seven transmembrane domain receptor signalling networks. *Br. J. Pharmacol.* **159**, 738–750 (2010).
40. P. H. Viollier, N. Sternheim, L. Shapiro, Identification of a localization factor for the polar positioning of bacterial structural and regulatory proteins. *Proc. Natl. Acad. Sci. U.S.A.* **99**, 13831–13836 (2002).
41. A. J. Hinz, D. E. Larson, C. S. Smith, Y. V. Brun, The *Caulobacter crescentus* polar organelle development protein PodJ is differentially localized and is required for polar targeting of the PleC development regulator. *Mol. Microbiol.* **47**, 929–941 (2003).
42. W. Zhao *et al.*, A circuit of protein-protein regulatory interactions enables polarity establishment in a bacterium. *bioRxiv* [Preprint] (2018). <https://doi.org/10.1101/503250> (Accessed 21 December 2018).
43. G. Ebersbach, A. Briegel, G. J. Jensen, C. Jacobs-Wagner, A self-associating protein critical for chromosome attachment, division, and polar organization in *Caulobacter*. *Cell* **134**, 956–968 (2008).
44. K. Lasker *et al.*, Selective sequestration of signalling proteins in a membraneless organelle reinforces the spatial regulation of asymmetry in *Caulobacter crescentus*. *Nat. Microbiol.* **5**, 418–429 (2020).
45. J. A. Holmes *et al.*, *Caulobacter* PopZ forms an intrinsically disordered hub in organizing bacterial cell poles. *Proc. Natl. Acad. Sci. U.S.A.* **113**, 12490–12495 (2016).
46. M. Bergé *et al.*, Modularity and determinants of a (bi-)polarization control system from free-living and obligate intracellular bacteria. *eLife* **5**, e20640 (2016).
47. P. D. Dahlberg *et al.*, Cryogenic single-molecule fluorescence annotations for electron tomography reveal in situ organization of key proteins in *Caulobacter*. *Proc. Natl. Acad. Sci. U.S.A.* **117**, 13937–13944 (2020).
48. A. Gahlmann *et al.*, Quantitative multicolor subdiffraction imaging of bacterial protein ultrastructures in three dimensions. *Nano Lett.* **13**, 987–993 (2013).
49. J. L. Ptacin *et al.*, Bacterial scaffold directs pole-specific centromere segregation. *Proc. Natl. Acad. Sci. U.S.A.* **111**, E2046–E2055 (2014).
50. G. R. Bowman *et al.*, *Caulobacter* PopZ forms a polar subdomain dictating sequential changes in pole composition and function. *Mol. Microbiol.* **76**, 173–189 (2010).
51. N. H. Bhat, R. H. Vass, P. R. Stoddard, D. K. Shin, P. Chien, Identification of ClpP substrates in *Caulobacter crescentus* reveals a role for regulated proteolysis in bacterial development. *Mol. Microbiol.* **88**, 1083–1092 (2013).
52. U. Jenal, T. Fuchs, An essential protease involved in bacterial cell-cycle control. *EMBO J.* **17**, 5658–5669 (1998).
53. M. J. Stallmeyer, K. M. Hahnenberger, G. E. Sosinsky, L. Shapiro, D. J. DeRosier, Image reconstruction of the flagellar basal body of *Caulobacter crescentus*. *J. Mol. Biol.* **205**, 511–518 (1989).
54. C. D. Mohr, U. Jenal, L. Shapiro, Flagellar assembly in *Caulobacter crescentus*: A basal body P-ring null mutation affects stability of the L-ring protein. *J. Bacteriol.* **178**, 675–682 (1996).
55. J. Yu, L. Shapiro, Early *Caulobacter crescentus* genes flilL and flilM are required for flagellar gene expression and normal cell division. *J. Bacteriol.* **174**, 3327–3338 (1992).
56. S. Ardisson, P. H. Viollier, Interplay between flagellation and cell cycle control in *Caulobacter*. *Curr. Opin. Microbiol.* **28**, 83–92 (2015).
57. A. Eletsky *et al.*, NMR structure of protein Yvyc from *Bacillus subtilis* reveals unexpected structural similarity between two PFAM families. *Proteins* **76**, 1037–1041 (2009).
58. M. Kalmokoff *et al.*, Proteomic analysis of *Campylobacter jejuni* 11168 biofilms reveals a role for the motility complex in biofilm formation. *J. Bacteriol.* **188**, 4312–4320 (2006).
59. S. Capdevila, F. M. Martínez-Granero, M. Sánchez-Conreras, R. Rivilla, M. Martín, Analysis of *Pseudomonas fluorescens* F113 genes implicated in flagellar filament synthesis and their role in competitive root colonization. *Microbiology (Reading)* **150**, 3889–3897 (2004).
60. K. McGee, P. Hörstedt, D. L. Milton, Identification and characterization of additional flagellin genes from *Vibrio anguillarum*. *J. Bacteriol.* **178**, 5188–5198 (1996).
61. B. Zhou *et al.*, The global regulatory architecture of transcription during the *Caulobacter* cell cycle. *PLoS Genet.* **11**, e1004831 (2015).
62. W. C. Nierman *et al.*, Complete genome sequence of *Caulobacter crescentus*. *Proc. Natl. Acad. Sci. U.S.A.* **98**, 4136–4141 (2001).
63. B. Ely, T. W. Ely, W. B. Crymes Jr, S. A. Minnich, A family of six flagellin genes contributes to the *Caulobacter crescentus* flagellar filament. *J. Bacteriol.* **182**, 5001–5004 (2000).
64. A. Weissborn, H. M. Steinmann, L. Shapiro, Characterization of the proteins of the *Caulobacter crescentus* flagellar filament. Peptide analysis and filament organization. *J. Biol. Chem.* **257**, 2066–2074 (1982).
65. A. C. Meisenzahl, L. Shapiro, U. Jenal, Isolation and characterization of a xylose-dependent promoter from *Caulobacter crescentus*. *J. Bacteriol.* **179**, 592–600 (1997).
66. J. Yan, L. Kurgan, DRNApred, fast sequence-based method that accurately predicts and discriminates DNA- and RNA-binding residues. *Nucleic Acids Res.* **45**, e84 (2017).
67. M. Milhausen, N. Agabian, *Caulobacter* flagellin mRNA segregates asymmetrically at cell division. *Nature* **302**, 630–632 (1983).
68. P. H. Viollier *et al.*, Rapid and sequential movement of individual chromosomal loci to specific subcellular locations during bacterial DNA replication. *Proc. Natl. Acad. Sci. U.S.A.* **101**, 9257–9262 (2004).
69. C. Kim, C. Y. Cheng, S. A. Saldanha, S. S. Taylor, PKA-I holoenzyme structure reveals a mechanism for cAMP-dependent activation. *Cell* **130**, 1032–1043 (2007).
70. I. Bosanac *et al.*, Structure of the inositol 1,4,5-trisphosphate receptor binding core in complex with its ligand. *Nature* **420**, 696–700 (2002).
71. M. Zhang, T. Tanaka, M. Ikura, Calcium-induced conformational transition revealed by the solution structure of apo calmodulin. *Nat. Struct. Biol.* **2**, 758–767 (1995).
72. B. Ely, Genetics of *Caulobacter crescentus*. *Methods Enzymol.* **204**, 372–384 (1991).
73. J. M. Schrader, L. Shapiro, Synchronization of *Caulobacter crescentus* for investigation of the bacterial cell cycle. *J. Vis. Exp.* (2015).
74. R. Paul *et al.*, Activation of the diguanylate cyclase PleD by phosphorylation-mediated dimerization. *J. Biol. Chem.* **282**, 29170–29177 (2007).
75. C. J. Wienken, P. Baaske, U. Rothbauer, D. Braun, S. Duhr, Protein-binding assays in biological liquids using microscale thermophoresis. *Nat. Commun.* **1**, 100 (2010).
76. S. A. Seidel *et al.*, Microscale thermophoresis quantifies biomolecular interactions under previously challenging conditions. *Methods* **59**, 301–315 (2013).
77. G. Karimova, J. Pidoux, A. Ullmann, D. Ladant, A bacterial two-hybrid system based on a reconstituted signal transduction pathway. *Proc. Natl. Acad. Sci. U.S.A.* **95**, 5752–5756 (1998).
78. J. Fei *et al.*, RNA biochemistry. Determination of *in vivo* target search kinetics of regulatory noncoding RNA. *Science* **347**, 1371–1374 (2015).
79. C. A. Bayas *et al.*, Spatial organization and dynamics of RNase E and ribosomes in *Caulobacter crescentus*. *Proc. Natl. Acad. Sci. U.S.A.* **115**, E3712–E3721 (2018).
80. M. Ovesný, P. Křížek, J. Borkovec, Z. Svindrych, G. M. Hagen, ThunderSTORM: A comprehensive imageJ plug-in for PALM and STORM data analysis and super-resolution imaging. *Bioinformatics* **30**, 2389–2390 (2014).
81. M. P. Backlund, R. Joyner, W. E. Moerner, Chromosomal locus tracking with proper accounting of static and dynamic errors. *Phys. Rev. E Stat. Nonlin. Soft Matter Phys.* **91**, 062716 (2015).